# Simple shear of metal sheets at high rates of strain

*Dedicated to Professor Franz Ziegler*
*on the occasion of His 60th birthday*

H. V. NGUYEN and W. K. NOWACKI (WARSZAWA)

THE TEST of dynamic (at high rates of strain) plane shear is discussed. Use is made of the new shear device in which the loading and displacements are controlled by the Split Hopkinson Pressure Bar acting in compression. This device allows to perform tests under the plane shear state in a specimen having the form of metal sheets. Simplified analytical solution of the boundary-value problem in the case of simple shear is prescribed. The analytical solution of the initial-boundary problem is compared with the experimental data.

## 1. Introduction

NUMERICAL SYSTEMS allow us to simulate the mechanical behaviour of thin-walled constructions, such as body of automobiles, buses, shells of wagons, air-planes, etc., subjected to the impact loading; required is the knowledge of the dynamical behaviour of thin sheets in which these constructions are made. Their mechanical characteristics are dependent on the metallurgical composition of the metal as well on the manner of its production. It is indispensable to have the experimental data concerning this specific form of material. Tests in the case of simple shear are very important for the experimental investigation of the constitutive equations of materials. These experiments are supplementary to other tests realized in the conditions of tension as well in the compression or in the pure shear.

Recently, a new shear device was used to perform tests on specimens having the form of slabs such as metal sheets [1]. The loading and the displacements of this device are controlled by a Split Hopkinson Pressure Bar (SHPB) acting in compression. The special device was used to transform the compression to simple plane shear. For thin sheets in dynamic simple plane shear tests, it is the only known method to obtain a very good homogeneity of the permanent strain field over the total length of the specimen, without the localization of deformations as in the case of torsion of thin-walled tubes [2, 3 and 13].

The analogous initial-boundary-value problem of simple shear was formulated in the case of finite strains. We consider the rate-independent constitutive relations for adiabatic process with combined isotropic-kinematic hardening at moderate pressures. The thermal expansion, the heat of elastic deformation and the heat of internal rearrangement are neglected. The analytical solution is compared with the experimental data. The performed numerical calculations enabled

the evaluation of the optimal dimensions of the specimen used in the case of dynamic loading.

## 2. Experiment

Figure 1 presents the principle of the shear device. The shear device consists of two coaxial cylindrical parts (the external part is tubular and the internal part is massive). Both cylinders are divided into two symmetrical parts, and between them the sheet in testing is fixed using screws of high strength – Fig. 2. Two bands of the specimen between the internal and external parts of the device are in plane shear when these cylinders move axially one toward the other. The width of these bands is 3 mm. Each band before test is rectangular and becomes very near parallelogram having the constant length and the constant height. The specimens can have different thickness. There are two kinds of specimens: one is made of the steel XES (chemical composition: C–50, Ni–25, Cr–18, Mn–189, Cu–23, Al–57, Si–4, P–17 in $10^{-3}$ volume percent, thickness 0.74 mm) and the other is of steel 1H18N9T (chemical composition: C–10, Mn–200, Si–80, P–5, S–3 Cr–180, Ni–80, thickness 0.5 mm).
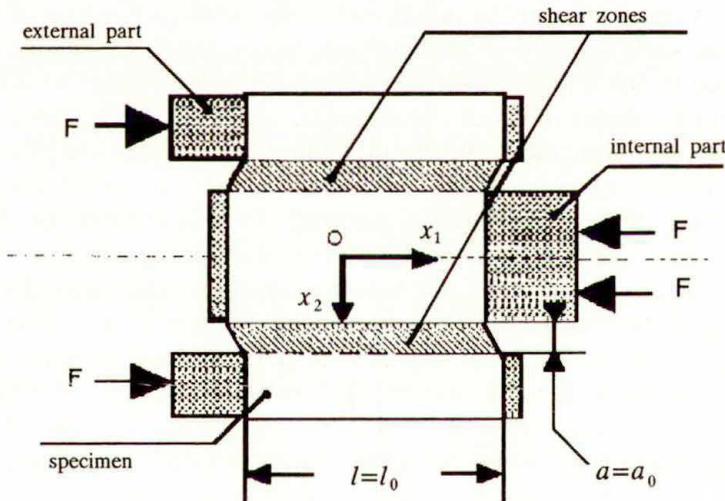


FIG. 1. Scheme of the shear device.

First, the system is tested under quasi-static loading for verifying the effectiveness. The presence of free bounds of specimen produces the heterogeneity of stress field because the stress vector normal to the free surfaces must be zero, therefore we have assumed that the dimensions of the perturbed zone are small compared to the dimensions of the specimen. This assumption is acceptable as shown in [1], where the mounting of the sheet is tested and the homogeneity of the field of deformation is observed. In general, we must take the ratio $a_0/l_0$
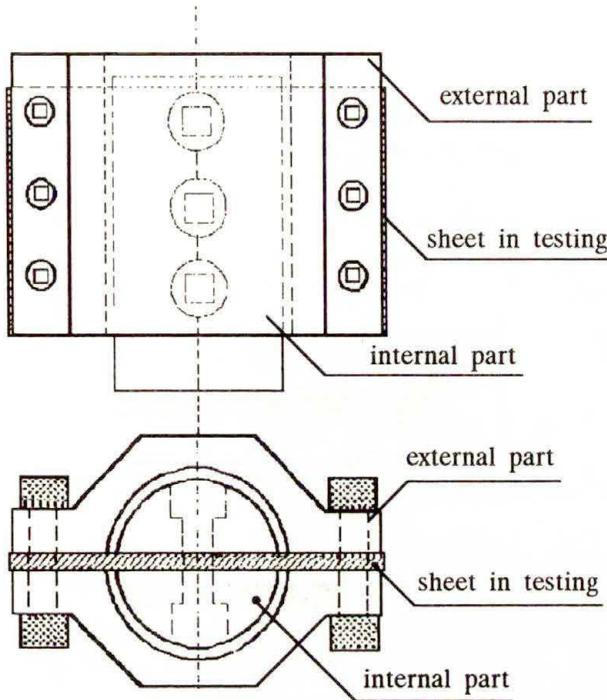
Fig. 2. Shear device in detail.

sufficiently small. It is shown in [8, 9] that when the ratio $a_0/l_0 \leq l/10$, the results of test are good for both static and dynamic cases. We take in our tests $a_0/l_0 = l/10$.

The dynamic test is similar but the loading is realized by the SHPB. The device with specimen is placed between two bars of the SHPB. In this case the mechanical impedance of the shear device and the SHPB must be the same to avoid the noise in the interface signal. The impulse is created by the third projectile bar: the usual compression technique. We have to register the input, the transmitted and the reflected impulse: $\varepsilon_i$, $\varepsilon_t$ and $\varepsilon_r$. The highest strain rate in the specimen can be obtained using only one bar of the SHPB system. We use the transmitted bar only and the shearing device is placed in the front of this bar. The projectile bar strikes directly the device. We have to register only the transmitted impulse $\varepsilon_t$ and the velocity of the projectile.

Measurement of quasi-static or dynamic deformation in the case of simple shear of the metal sheets is not very simple. The specimen is deformed not only between the grips, in the gauge section, the part under the grips is partially deformed too. The transversal strike lines, marked on the specimen before the test, for example the line $AB$ shown in the Fig. 3 a becomes after deformation the curve $AB'$ with the strike sections $Aa$, $b'c'$ and $dB'$. These curves observed under the optical microscope are shown by the photo – Fig. 3 b.
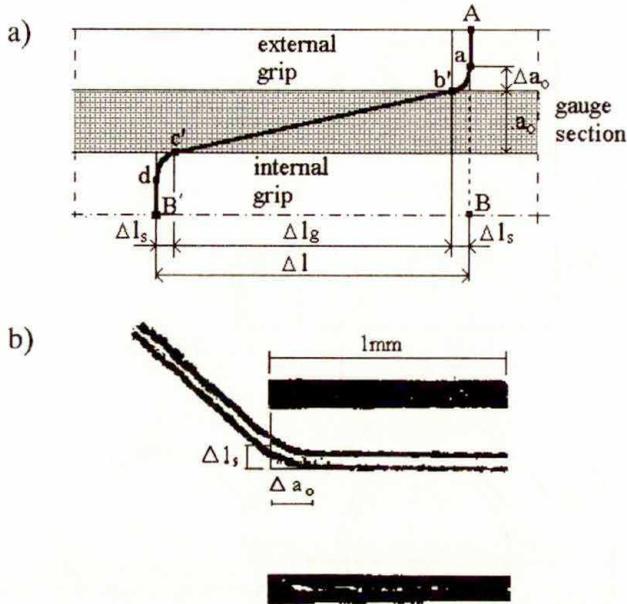
FIG. 3. Deformation in simple shear of the sheet, in the gauge section and under the grips:
a) scheme, b) observed under the optical microscope.

Relative displacement of external and internal parts of shear device $\Delta l$ is easy to measure in the case of quasi-static deformation (in the testing machine) as well in the case of dynamic deformation – in SHPB system. It is a sum of two terms: $\Delta l = \Delta l_g + 2\Delta l_s$, where $\Delta l_g$ corresponds to the deformation in the simple shear defined as $\gamma = \Delta l_g / a_0$, and $\Delta l_s$ correspond to the value of sliding under the grips. It was assumed that, in the case of simple plane shear, there is no change in the cross-section: $S_E = $ const ($S_E = l_0 d$; where $d$ is the thickness of the specimen). Then the mean shear stress is defined by $\sigma_{12} = F/S_E$.

The estimations of the sliding value under the grips $\Delta l_s$ can be obtained in the quasi-static test of loading-unloading. After this test, the permanent deformation of the specimen can be measured using the optical microscope. Comparisons of this measure with those obtained by an extensometer at the end of the unloading process yields the value of $\Delta l_s$, for the given range of deformation $\gamma$.

We can notice that the shear device can be also deformed during the test. It is desirable that the measurement of deformation should be performed as near as possible to the gauge section. In this case the best is the local optical measure of deformation made by the CCD camera, with simultaneous treatment of the picture. The principle of this method is described in [14]. Using this method, we can determine the shear deformation of the specimen with the accuracy of the order of $2 \cdot 10^{-5}$. In [14] it is proved that the measurement by the relative displacement of the grips is also good, on condition that the deformation of the specimen under the grips is taken into consideration.

In the axis of Fig. 1 the stress tensor has the following components: $\sigma_{11}$, $\sigma_{22}$ and $\sigma_{12}$. The presence of $\sigma_{11}$ and $\sigma_{22}$ is due to the fact that the distance between two parts of the shear device is constant during experiment i.e. $a = a_0 = $ const. The strain tensor has only one non-zero component $\varepsilon_{12} = \gamma$. In this test, large deformations can be obtained without localisation of the deformation, contrary to the case of torsion of thin cylindrical specimens [2, 3 and 13], for example. The specimens deformed quasi-statically or dynamically to $70 - 90\%$ and observed under the optical microscope, have a similar structure. The transversal lines marked before the test on the specimens, on the gauge section, remain parallel after the test. This fact indicates that the deformation is homogeneous in the considerable part of the specimen. We have assumed that the dimensions of the perturbed zone are small compared to the dimensions of the specimen. The exceptional qualities of the homogeneity of the residual strain field show that the simplified analysis can be used in the zone of plastic deformations.
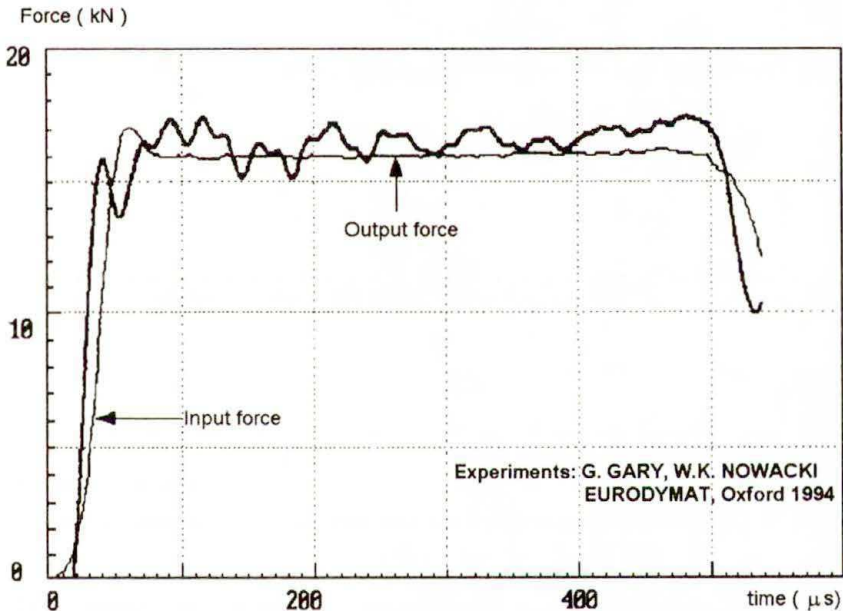


FIG. 4. Input and output forces measured in the experiment.

In the analysis, we must take into account that the loading of the specimen is not instantaneous. The loading compression wave must take some time to travel from one end to the other end of the device. However, we have in our tests very good equilibrium of forces on two sides of the shear device, see Fig. 4. We observe that the input force and the output are very similar in shape, neglecting the small oscillations of the input force. So, in the simplified analysis we suppose that the loading is homogeneous and we proceed as in the case of quasi-static loading. Knowing the velocities on bounds of the shear device, we can find the

displacements. The force is taken to be equal to the mean value of the input and output forces.

The sensibility to the rate of deformation in compression and in the simple shear is presented in Fig. 5. The experiments made on the XES steel at low and moderate strain rate (quasi-static test in compression and dynamic compression test using SHPB system) are performed by G. Gary and described in [1]. These results are completed by investigations in dynamic simple shear. The diagrams in the Fig. 5 present the variation of the maximal stress versus logarithmic rate of deformation, for different kinds of experiments mentioned above.

Maximal stress (MPa)
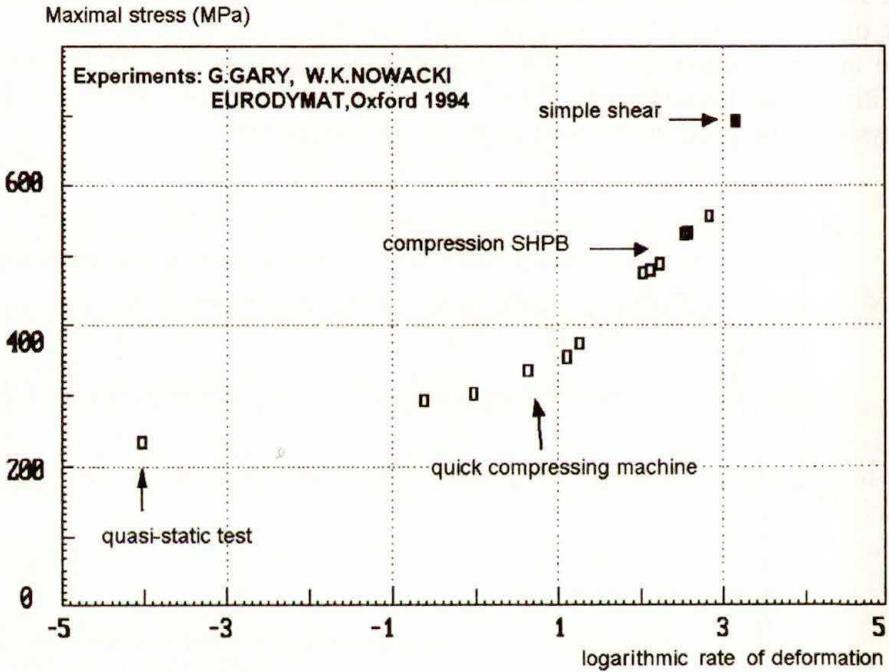


FIG. 5. Comparison of the simple shear test with the simple compression test [1].

In the paper [11] the quasi-static tests concerning the behaviour of 1H18N9T steel are discussed. The temperature field due to deformation is simultaneously registered. The goal of this paper was to obtain the mechanical curves as well as the temperature distributions in the shear regions. A change of temperature of the surface of these regions has been observed by the thermovision camera coupled with a system of data acquisition and conversion. The infrared radiation emitted by shear paths was measured. The results obtained enable us to present the temperature changes of the specimens subjected to the shear test with different rates of deformation, as well as to describe the macroscopic shear band developing at higher deformations. Finally, the experimental results were compared with the results of numerical simulations presented in Sec. 5 of the present paper.

## 3. Theoretical simple shear analysis

The simple shear in the direction $e_1$ of the coordinate system $(e_1, e_1)$ is defined by the relations

(3.1)
$$u_2 = u_3 = 0,$$
$$v_2 = v_3 = 0,$$

where $\gamma = \text{tg}\,\phi$ (cf. Fig. 6) and $\dot{\gamma}$ are the plastic shear strain and shear strain
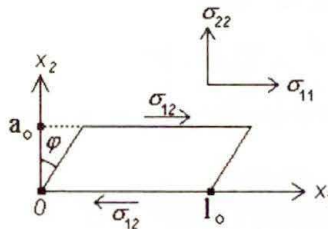


FIG. 6. Scheme of simple shear.

rate, respectively. From the velocity field $v$, the velocity gradient $V$, the rate of deformation $D$ and the material spin $\omega$ can be determined in the system $(e_1, e_1)$ as

(3.2)
$$V = \frac{\dot{\gamma}}{2}\begin{pmatrix} 0 & 1 \\ 0 & 0 \end{pmatrix}, \qquad D = \frac{\dot{\gamma}}{2}\begin{pmatrix} 0 & 1 \\ 1 & 0 \end{pmatrix}, \qquad \omega = \frac{\dot{\gamma}}{2}\begin{pmatrix} 0 & 1 \\ -1 & 0 \end{pmatrix}.$$

The Cauchy stress tensor $\sigma$ and the back stress $\Pi$ have the non-zero components

(3.3)
$$\sigma = \begin{pmatrix} \sigma_{11} & \sigma_{12} \\ \sigma_{21} & \sigma_{22} \end{pmatrix}, \qquad \Pi = \begin{pmatrix} \pi_{11} & \pi_{12} \\ \pi_{21} & \pi_{22} \end{pmatrix}.$$

Using the constitutive relations for adiabatic process for rate-independent materials with combined isotropic-kinematic hardening at moderate pressures, when the thermal expansion, the heat of elastic deformation and the heat of internal rearrangement are neglected, we obtain the following constitutive equations [10]

(3.4)
$$\check{T} = \beta L\,D - \frac{3j\mu\beta D\cdot(\overline{T} - \Pi)}{\sigma_Y^2 \mathcal{H}}[(\overline{T} - \Pi) + P],$$

$$j = \begin{cases} 1 & \text{if } f = 0 \text{ and } D\cdot(\overline{T} - \Pi) \geq 0, \\ 0 & \text{if } f = 0 \text{ and } D\cdot(\overline{T} - \Pi) < 0, \quad \text{or } f < 0, \end{cases}$$

where $\beta = \varrho_0/\varrho$ is the ratio of densities in the reference and actual configurations, $T = \beta\sigma$, $\check{T} = \dot{T} - \omega T + T\omega$ is the Zaremba–Jaumann rate, $\overline{T}$ is the deviatoric

part of **T**, **L** is the fourth order tensor of elastic moduli, $\mu$ is the Lamé constant and $f$ is the Huber–Mises yield criterion

(3.5)
$$f = \frac{3}{2}(\overline{\mathbf{T}} - \mathbf{\Pi}) \cdot (\overline{\mathbf{T}} - \mathbf{\Pi}) - \sigma_Y^2(\vartheta, \alpha) = 0,$$

where $\sigma_Y$ is the yield stress in simple tension, $\vartheta$ is the temperature and $\alpha$ corresponds to the size of the yield surface

(3.6)
$$\dot{\alpha} = (\overline{\mathbf{T}} - \mathbf{\Pi}) \cdot \mathbf{D^P}.$$

The shift of the yield surface is represented here by the back stress $\mathbf{\Pi}$ for which the evolution law has the form of linear kinematic hardening

(3.7)                      ████████████

where $c = $ const and $\mathbf{D^P}$ is the plastic rate of deformation. The change in the temperature is described as

(3.8)                 █████████████████

$c_v$ is specific heat at constant volume; the first term on the right-hand side of (3.8) represents the rate of energy dissipation and, therefore, $\pi < 1$. For numerous metals $\pi$ takes the value from 0.02 to 0.1 [10]. In Eq. (3.4) $\mathcal{H}$ is the hardening function

$$\mathcal{H} = 1 + \frac{c}{2\mu\beta} + \frac{1}{6\mu\beta}\frac{\partial(\sigma_Y^2)}{\partial\alpha} + \frac{(1-\pi)}{6\mu\beta\varrho_0 c_v}\frac{\partial(\sigma_Y^2)}{\partial\vartheta}$$

and tensor **P** is obtained by expressing the term $(\boldsymbol{\omega}_p\mathbf{T} + \mathbf{T}\boldsymbol{\omega}^p)$ as a function of $\mathbf{D^P}$ where $\boldsymbol{\omega}^p$ is the plastic spin.

The equation for plastic spin can be assumed, according to Dafalias [6], Paulun and Pęcherski [7] and others, in the following form

(3.9)
$$\boldsymbol{\omega}^p = \eta(\mathbf{\Pi}\,\mathbf{D^P} - \mathbf{D^P}\mathbf{\Pi}),$$

where $\eta$ may depend on the invariants of $\mathbf{D^P}$ and $\mathbf{\Pi}$.

In the case of plane simple shear we have $\beta = 1$ and the equations above lead to

(3.10)
$$\dot{\sigma}_{11} - \dot{\gamma}\sigma_{12} = -\frac{3j\mu}{\sigma_Y^2\mathcal{H}}\left[\dot{\gamma}(\sigma_{12} - \pi_{12})\right]\left[(\sigma_{11} - \pi_{11}) + \frac{\eta}{\mu}\mathcal{M}\sigma_{12}\right],$$

$$\dot{\sigma}_{12} - \dot{\gamma}\sigma_{11} = \mu\dot{\gamma} - \frac{3j\mu}{\sigma_Y^2\mathcal{H}}\left[\dot{\gamma}(\sigma_{12} - \pi_{12})\right]\left[(\sigma_{12} - \pi_{12}) - \frac{\eta}{\mu}\mathcal{M}\sigma_{11}\right],$$

$$\dot{\pi}_{11} - \dot{\gamma}\pi_{12} = \frac{3jc}{\sigma_Y^2\mathcal{H}}\left[\dot{\gamma}(\sigma_{12} - \pi_{12})\right](\sigma_{11} - \pi_{11}),$$

$$\dot{\pi}_{12} - \dot{\gamma}\pi_{11} = \frac{3jc}{\sigma_Y^2\mathcal{H}}\left[\dot{\gamma}(\sigma_{12} - \pi_{12})\right](\sigma_{12} - \pi_{12});$$

here $\sigma_{11} = -\sigma_{22}$, $\pi_{11} = -\pi_{22}$, and

(3.11) $$\mathcal{M} = [\pi_{11}(\sigma_{12} - \pi_{12}) - \pi_{12}(\sigma_{11} - \pi_{11})].$$

We use here the relation for the function $\eta$ occurring in the expression of plastic spin (3.9), in the form proposed in the papers [6, 7, 15 and 16]:

(3.12) $$\eta = \frac{3}{\left[\left(\frac{3c}{2}\right)^2 + \frac{3c}{2}\left(\frac{3}{2}\Pi \cdot \Pi\right)^{1/2}\right]^{1/2}}.$$

The Huber–Mises yield criterion (3.5) is

(3.13) $$\begin{aligned} f &= \frac{3}{2}(\bar{\sigma} - \Pi) \cdot (\bar{\sigma} - \Pi) - \sigma_Y^2 \\ &= 3\left[(\sigma_{11} - \pi_{11})^2 + (\sigma_{12} - \pi_{12})^2\right] - \sigma_Y^2(\alpha, \vartheta) = 0, \end{aligned}$$

and in the equations (3.10) we have

(3.14) $$j = \begin{cases} 1 & \text{if } f = 0 \text{ and } \dot{\gamma}(\sigma_{12} - \pi_{12}) \geq 0, \\ 0 & \text{if } f = 0 \text{ and } \dot{\gamma}(\sigma_{12} - \pi_{12}) < 0, \quad \text{or } f < 0. \end{cases}$$

The change in the temperature $\vartheta$ is described by

(3.15) $$\varrho_0 c_v \dot{\vartheta} = j\frac{(1 - \pi)[\dot{\gamma}(\sigma_{12} - \pi_{12})]}{\mathcal{H}}.$$

The hardening function $\mathcal{H}$ now is

(3.16) $$\mathcal{H} = 1 + \frac{c}{2\mu} + \frac{1}{6\mu}\frac{\partial(\sigma_Y^2)}{\partial\alpha} + \frac{(1 - \pi)}{6\mu\varrho_0 c_v}\frac{\partial(\sigma_Y^2)}{\partial\vartheta}.$$

In case of elasticity $j = 0$ and Eqs. (3.10) reduce to

(3.17) $$\begin{aligned} \dot{\sigma}_{11} - \gamma\sigma_{12} &= 0, \\ \dot{\sigma}_{12} - \gamma\sigma_{11} &= \mu\dot{\gamma}, \\ \dot{\pi}_{11} - \gamma\pi_{12} &= 0, \\ \dot{\pi}_{12} + \gamma\pi_{11} &= 0. \end{aligned}$$

Under the initial conditions that for $\gamma = 0$, stresses $\sigma_{11} = \sigma_{12} = \pi_{11} = \pi_{12} = 0$, we have the analytical solution:

(3.18) $$\begin{aligned} \sigma_{11} &= \mu(1 - \cos\gamma), \\ \sigma_{12} &= \mu\sin\gamma, \\ \pi_{11} &= 0, \\ \pi_{12} &= 0. \end{aligned}$$

The stress-shear strain relations, in the range of elastic deformations, are shown in the Fig. 7, with $\mu = 8\cdot10^4$ MPa. The contribution of normal stress $\sigma_{11}$ and $\sigma_{22}$ is very small in comparison with that of the stress component $\sigma_{12}$.
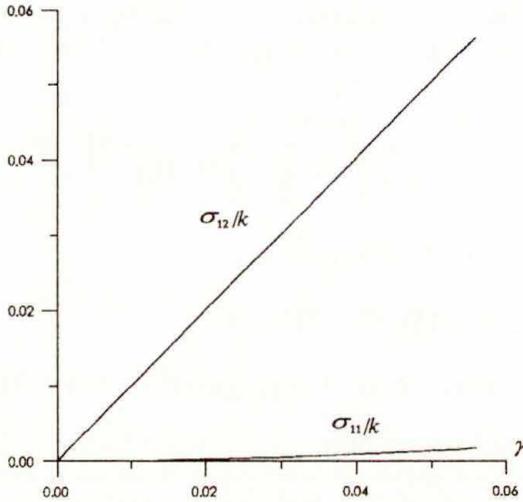


FIG. 7. Shear stress $\sigma_{12}$ and normal stress $\sigma_{11}$ vs. shear strain: elastic material.

We can show that in the case of plasticity with kinematic hardening, we also obtain analytical solutions. Then $\sigma_Y = $ const and now from (3.16) we have

(3.19)

Introducing the new variable $\phi$ satisfying the yield condition

$$(3.20) \qquad \begin{aligned} \sigma_{11} - \pi_{11} &= (1/\sqrt{3})\sigma_Y \cos\phi, \\ \sigma_{12} - \pi_{12} &= (1/\sqrt{3})\sigma_Y \sin\phi, \end{aligned}$$

the relation between $\phi$ and $\gamma$ is now the following:

$$(3.21) \qquad \frac{\sqrt{a^2-1}\tan\dfrac{\phi}{2} + (a-1)}{\sqrt{a^2-1}\tan\dfrac{\phi}{2} - (a-1)} \exp\left(-\sqrt{a^2-1}\gamma\right) = C,$$

where $a = \mu/k_0$, $k_0 = \sigma_Y/\sqrt{3}$ is the yield value in shear and

$$C = \frac{\sqrt{a^2-1}\tan\dfrac{\phi^*}{2} + (a-1)}{\sqrt{a^2-1}\tan\dfrac{\phi^*}{2} - (a-1)} \exp\left(-\sqrt{a^2-1}\gamma^*\right),$$

and where $\gamma^*$ and $\phi^*$ are described by the formula $\sin(\gamma^*/2) = k_0/2\mu$ and $\tan(\gamma^*/2) = \operatorname{ctg}\phi^*$.

The back stress $\pi_{11}$ satisfies the equation

(3.22)
$$\frac{d\pi_{11}}{d\phi} - \pi_{11}\frac{\tan\phi}{a\cos\phi - 1} = \frac{c}{2\mathcal{H}}\frac{\sin\phi\cos\phi}{a\cos\phi - 1}$$

hence we can calculate $\pi_{12}$ by the formula

(3.23)
$$\pi_{12} = \pi_{11}\tan\phi.$$

We find $\sigma_{11}$, $\sigma_{12}$ from (3.20) and finally we determine

(3.24)
$$\pi_{11} = \frac{c}{2\mathcal{H}}(\cos\phi - \cos\phi^*)\frac{\cos\phi}{(1 - a\cos\phi)},$$
$$\pi_{12} = \frac{c}{2\mathcal{H}}(\cos\phi - \cos\phi^*)\frac{\sin\phi}{(1 - a\cos\phi)},$$
$$\sigma_{11} = \frac{c}{2\mathcal{H}}(\cos\phi - \cos\phi^*)\frac{\cos\phi}{(1 - a\cos\phi)} + k_0\cos\phi,$$
$$\sigma_{12} = \frac{c}{2\mathcal{H}}(\cos\phi - \cos\phi^*)\frac{\sin\phi}{(1 - a\cos\phi)} + k_0\sin\phi.$$

The analytical solution for the normal and tangential components of the back stress tensor $\pi_{11}$ and $\pi_{12}$ could be used directly to evaluate the function $\eta$ given in (3.12).
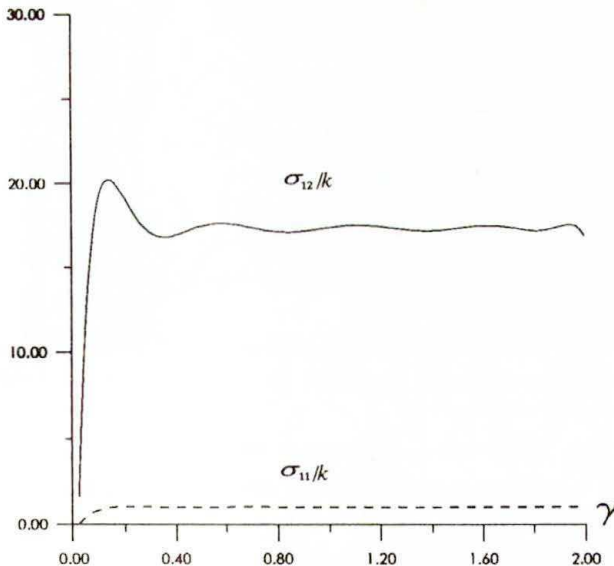


FIG. 8. Shear stress $\sigma_{12}$ and normal stress $\sigma_{11}$ vs. shear strain for kinematic hardening.

Now, we can determine the stress – shear strain relations in the range of non-elastic deformations. Solutions for stresses $\sigma_{11}$ and $\sigma_{12}$ in dimensionless form vs. shear strain $\gamma$, illustrated in Fig. 8, are obtained for kinematic hardening, using the same material properties as in the paper [12], namely: $\mu = 8 \cdot 10^4$ MPa, $c = 5333, 33$ MPa, $k_0/\mu = 0.0577$. Results of calculations for kinematic hardening are similar to those obtained in the paper [12]. In the case of large plastic deformations, the ratios $\sigma_{11}/\sigma_{12}$ and $\sigma_{22}/\sigma_{12}$ are much higher than in the case of small elastic deformations – cf. Fig. 7.

## 4. Metallurgical and thermomechanical observations

A portion of the gauge length of the specimen submitted to the simple shear test, with high strain rate, is shown in the Fig. 9. The shear deformation is of the order of 73%. An essential feature is the formation of the tangled structure and dislocations cells. Their elongation and arrangement tend to be aligned along the shear direction. In several grains the micro-bands of shear, parallel to the direction of $x_1$ axis are observed.



direction
of
traction
( $x_1$ axis )
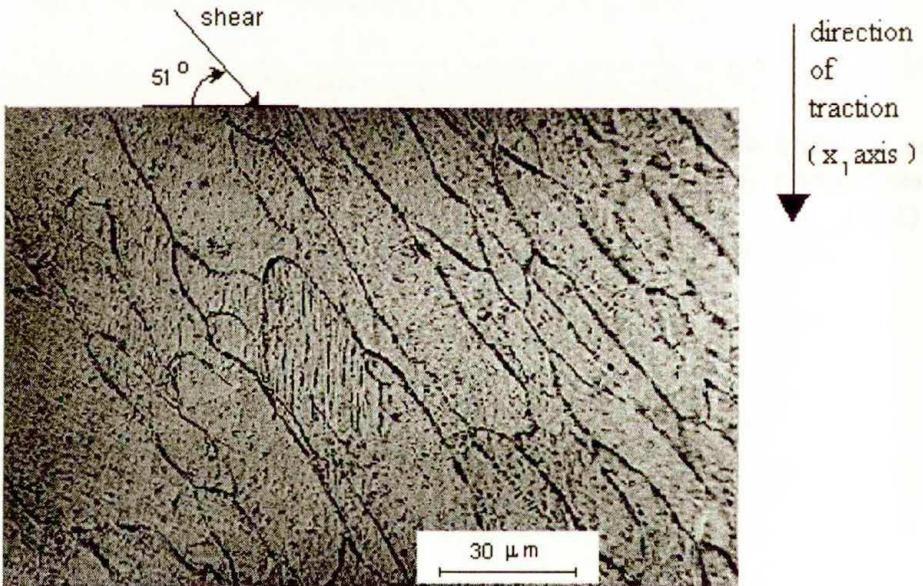
FIG. 9. Macro- and micro-bands of shear in the specimen subjected to simple shear.

At the very high strain rate, the shear macro-bands are observed. We can suppose that it is a critical strain at which the shear localization occurs. Before arriving at the critical strain, the deformation goes uniformly over the whole gauge length of the specimen. The work-hardening results from the creation, multiplication and interaction of the dislocations. In this case, a small part of the

work of plastic deformation is stored in the material as elastic strain energy (about 6% cf. [13]) and the remaining part is converted into heat. In the paper [11] the temperature field due to plastic deformation is measured by the thermovision camera. With this technique, it is possible to evaluate the stored energy due to simple shear in the case of large deformations. The shear macro-bands are observed in the case of quasi-static deformations.

$1\bar{2}1$
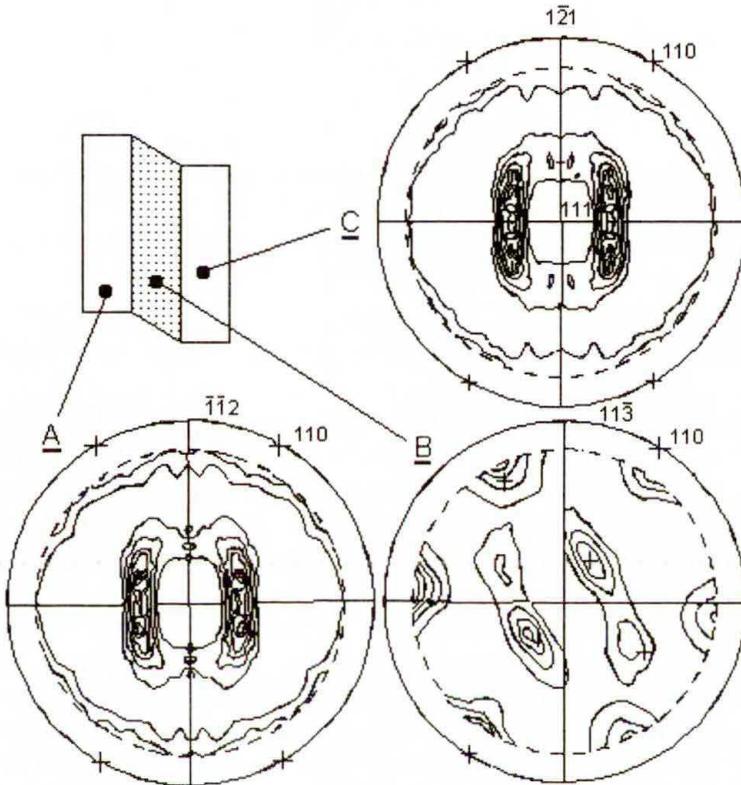


FIG. 10. a) and c) initial texture of the sheet (zones undeformed under grips), b) texture measured in the deformed zone after simple shear – permanent deformation 73%.

The initial texture is illustrated in Fig. 10 a and Fig. 10 c. The texture evolution after the large deformation of the order of 73% is shown in the Fig. 10 b, which shows a clear loss of orthotropy with respect to the initial reference frame. The final textures found in different points of the shear zones after simple shear are very similar.

## 5. Numerical simulations of the experiment

The program of finite element method was used to the numerical simulations of the formulated problem of quasi-static and dynamic simple shear of thin

sheets. We assume the initial and boundary conditions similar to those used in the experiment.

**A.** In the case of quasi-static loading, the boundary conditions have the following form:

In fixed ends of specimen (under grips) – cf. Fig. 6:

$$
(5.1) \quad
\begin{aligned}
u_1(x_1, x_2, t)\big|_{x_2=0} &= u_2(x_1, x_2, t)\big|_{x_2=0} = 0, \\
v_1(x_1, x_2, t)\big|_{x_2=a_0} &= v_0 \quad \text{and} \quad u_2(x_1, x_2, t)\big|_{x_2=a_0} = 0,
\end{aligned}
$$

where $v_0$ is the velocity of the testing machine in traction. In this case, the sliding of material under the grips is neglected.

At the free ends of the specimen (for $x_1 = 0$ and $x_1 = l_0$) we have:

$$
(5.2) \quad \sigma_{12}(x_1, x_2, t)\Big|_{\substack{x_1=0 \\ x_1=l_0}} = \sigma_{11}(x_1, x_2, t)\Big|_{\substack{x_1=0 \\ x_1=l_0}} = -\sigma_{22}(x_1, x_2, t)\Big|_{\substack{x_1=0 \\ x_1=l_0}} = 0.
$$

**B.** In the case of dynamic deformations, conditions (5.1) must be replaced by conditions of balance of forces in the contact between the specimen and the measuring bars. We should remember that the shear device and bars of SHPB system have identical mechanical impedances. At the same time, a simplifying assumption is introduced, and the process of waves propagation in the specimen is neglected.

With a view to a perfect equilibrium of input and output forces and quasi-constant value of the time period $50\,\mu s < t < 500\,\mu s$ – cf. Fig. 5, we can treat our problem as quasi-static. The amplitude of loading is determined from the dynamic experiment. We assume that in the contact between the specimen and measuring bars, the force is constant in time, cf. Fig. 5, and equal to $F_{max}$. The boundary conditions (4.1) take the form:

$$
(5.3) \quad \sigma_{12}(x_1, x_2, t)\Big|_{x_2=0} = -F_{max}/S_E \quad \text{and} \quad u_2(x_1, x_2, t)\Big|_{\substack{x_2=0 \\ x_2=a_0}} = 0.
$$

We assume the homogeneous zero initial conditions.

In the finite element method the rectangular mesh is introduced. Deformation of the mesh in time is determined. At the same time, the components of the stress tensor $\sigma_{12}$ and $\sigma_{22} = -\sigma_{11}$, the stress intensity $\sigma_i = (3/2 s_{ij} s_{ij})^{1/2}$ and the equivalent strain $e_i = (2/3 \varepsilon_{ij}^p \varepsilon_{ij}^p)^{1/2}$ are determined. First, the numerical simulation was made for the quasi-static loading of the sheet made of the steel 1H18N9T, with $\mu = 8 \cdot 10^4$ MPa, $\varrho = 7.8$ g/cm$^3$ and $\sigma_y = 280$ MPa.

Results of numerical simulation in the specimen subjected to quasi-static simple shear are shown in the Fig. 11. The equivalent deformation field is shown

shear strain 10.2 %

shear strain 13.2 %

shear strain 33.2 %

[FIG. 11]

shear strain 54.3 %

shear strain 74.1 %

shear strain 91.2 %
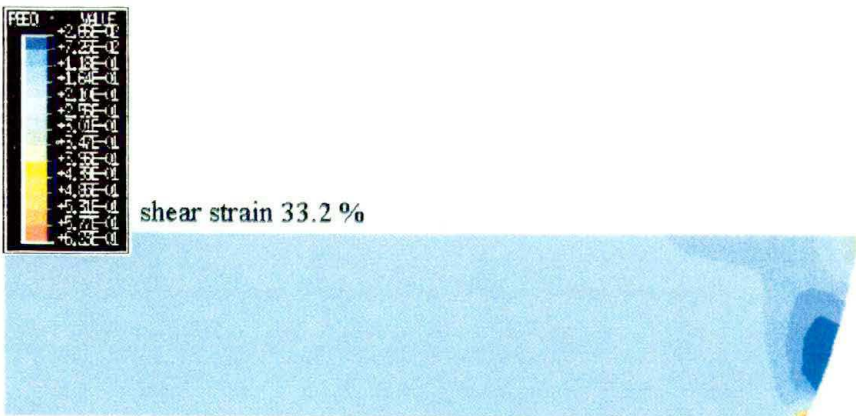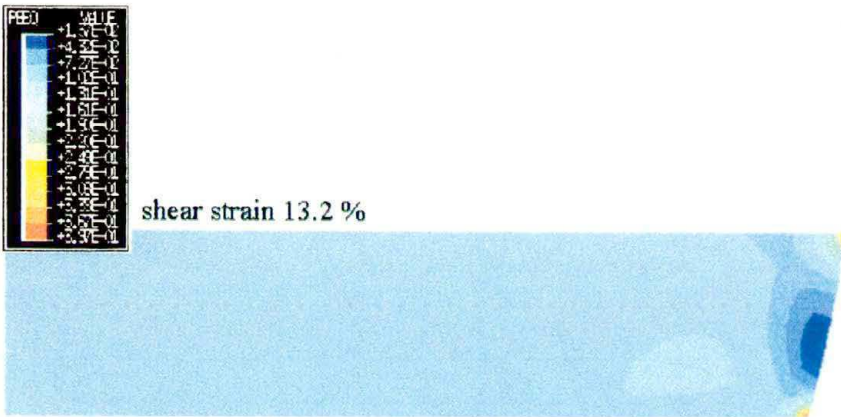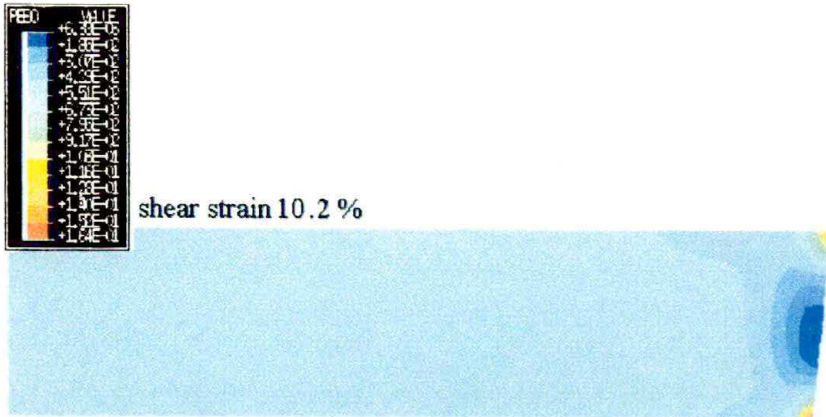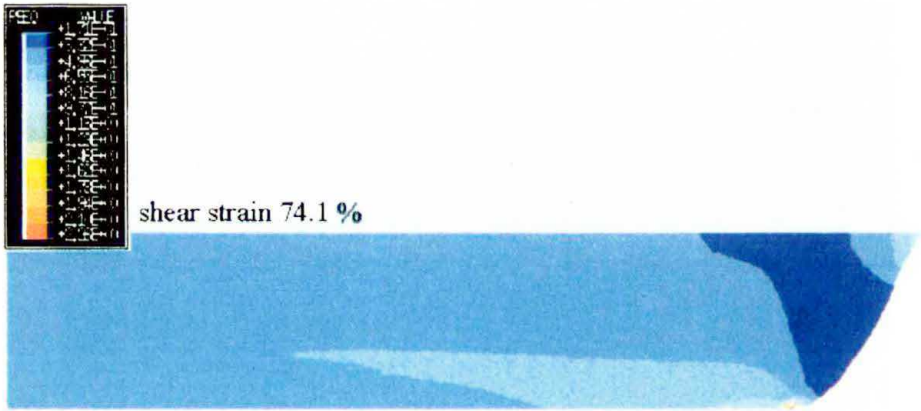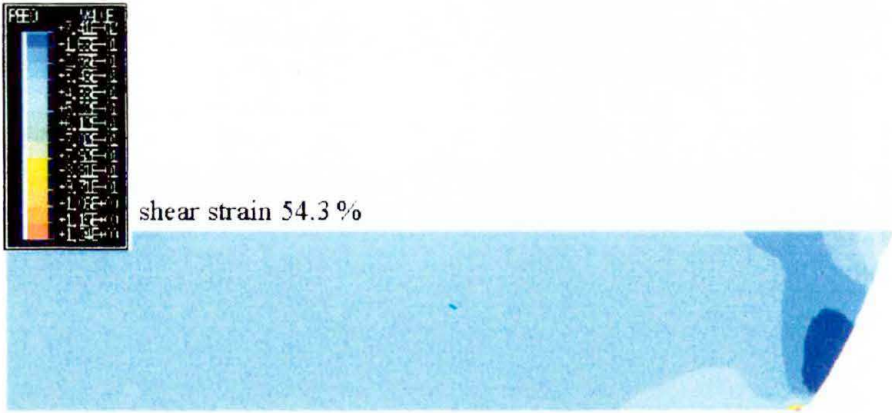
FIG. 11. Numerical simulation. Equivalent deformation.

for one half of the shear zone of the specimen, in view of the symmetry of deformation process with respect to the axis $x_2$ – cf. Fig. 1. Successive sequences are presented for different values of shear strain defined as $\gamma = \Delta l(t)/a_0$, from $\gamma = 10.2\%$ to $\gamma = 91.2\%$. We observe for example the heterogeneity of the strain and stress fields at the free ends of the specimen, at the distance less than 1.7% (accurate to 0.01% of deformation) of the total length when the strain is 30%, and less than 6.6% of the total length when the strain is 70%, exactly as in the experiments.

The performed numerical calculations enabled the evaluation of the optimal dimensions of the specimen.

## 6. Conclusions

Considerable homogeneity of the permanent strain field at finite deformations over the total length of the specimens is observed in experiments and in the results of simulation. The proposed method is the only known test providing, in the case of a thin sheet, homogeneous stress and strain fields in both the dynamic and static tests. They can be used to verify the constitutive relations proposed in [10]. Simple shear test is particularly attractive, since the application of this type of loading path can result in large strains without the occurrence of plastic instability. The advantages of the method in the case of static deformation were discussed widely in [5]. The thermo-mechanical coupling was described in the paper [11].

### References

1. G. GARY and W.K. NOWACKI, *Essai de cisaillement plan appliqué à des tôles minces*, J. de Physics IV, Colloque C8, Supplément au J. de Physic III 4, pp. 65–70, 1994.

2. K.A. HARTLEY, J. DUFFY and R.H. HAWLEY, *Measurement of the temperature profile during shear band formation in steels deforming at high strain rates*, J. Mech. Phys. Solids, **35**, 3, pp. 283–301, 1986.

3. A. MARCHAND and J. DUFFY, *An experimental study of the formation process of adiabatic shear bands in structural steel*, J. Mech. Phys. Solids, **36**, 3, pp. 251–283, 1988.

4. B. BACROIX and ZAIQIAN HU, *Texture evolution induced by strain path changes in low carbon steel sheets*, Metallurgical and Materials Trans. A, **26 A**, pp. 601–613, March 1995.

5.  B. Bacroix, P. Genevois and C. Teodosiu, *Plastic anisotropy in low carbon steels subjected to simple shear with strain path changes*, Eur. J.Mech., A/Solids, **13**, 5, pp. 661–675, 1994.

6.  Y.F. Dafalias, *A missing link in the macroscopic constitutive formulation of large plastic deformations*, [in:] Plasticity Today, pp. 135–151, A. Sawczuk, G. Bianchi [Eds.], Elsevier, 1985.

7.  J.E. Paulun and R. Pęcherski, *On the relation for plastic spin*, Arch. Appl. Mech., **62**, pp. 376–385, 1992.

8.  E.F. Rauch and C. G'Sell, *Flow localization induced by a change in strain path in mild steel*, Material Sci. and Engng., (A111), 71, 1989.

9.  A. Tourabi, B. Wack, P. Guélin, D. Favier, P. Pegon and W.K. Nowacki, *Remarks on an experimental plane shear test and on an anisotropic elastic-plastic theory*, Technical Report, SMIRT, 1993, Stuttgart, August 15-20, Elsevier Sci. Publ., 1993.

10.  Nguyen Huu Viem, *Isothermal and adiabatic flow laws of metallic elastic-plastic solids at finite strains and propagation of acceleration waves*, Arch. Appl. Mech., **44**, 5-6, pp. 595–602, 1992.

11.  P.S. Gadaj, W.K. Nowacki and E. Pieczyska, *Changes of temperature during the simple shear test of stainless steel*, Arch. Mech., **48**, 4, 1996.

12.  L. Szabo and M. Balla, *Comparison of some stress rates*, Int. J.Solids Structures, **25**, 3, pp. 279–297, 1989.

13.  Y.B. Xu, Y.L. Bai, Q. Xue and L.T. Shen, *Formation, microstructure and development of the localized shear deformation in low-carbon steel*, Acta Mater., **44**, 5, pp. 1917–1926, 1966.

14.  P.Y. Manach, *Etude du comportement thermomécanique d'alliages à mémoire de forme NiTi*, Doctoral Thesis, Institut National Polytechnique de Grenoble, 1993.

15.  J.E. Paulun and R.B. Pęcherski, *Study of corotational rates for kinematic hardening in finite deformation plasticity*, Arch. Mech., **37**, 6, pp. 661–677, 1985.

16.  R.B. Pęcherski, *Model of plastic flow accounting for the effects of shear banding and kinematic hardening*, ZAMM, Z. Angew. Math. Mech., **75**, pp. S 203–204, 1995.

INSTITUTE OF FUNDAMENTAL TECHNOLOGICAL RESEARCH
POLISH ACADEMY OF SCIENCES

e-mail: wnowacki@ippt.gov.pl